Int. J. Electrochem. Sci., 10 **(2015)** 823 - 837

International Journal of
ELECTROCHEMICAL
SCIENCE
www.electrochemsci.org

Experimental and Computational Evaluation of 3-indolebutyric Acid as a Corrosion Inhibitor for Mild Steel in Sulfuric Acid Solution

Jianhong Tan[1,*], *Lei Guo*[2], *Tangman Lv*[2], *Shengtao Zhang*[2]

[1] School of Chemistry and Chemical Engineering, Yangtze Normal University, Chongqing 408100, China
[2] School of Chemistry and Chemical Engineering, Chongqing University, Chongqing 400044, China
[*]E-mail: cqtanjc@163.com

Received: 25 October 2014 / *Accepted:* 19 November 2014 / *Published:* 2 December 2014

The inhibition effect of 3-indolebutyric acid (IBA) on the corrosion of mild steel in 0.1 mol L^{-1} H_2SO_4 solution was investigated using weight loss and electrochemical measurements. The polarization curves indicated that IBA behaved as a mixed-type inhibitor, affecting both cathodic and anodic corrosion currents. The absorption of IBA was found to obey the Langmuir adsorption isotherm. Quantum chemical parameters such as the highest occupied molecular orbital energy (E_{HOMO}), the lowest unoccupied molecular orbital energy (E_{LUMO}), Hirshfeld charges, dipole moment (μ), and the fraction of electrons transferred (ΔN), were calculated. Furthermore, Monte Carlo simulation studies were applied to search for the best configurational space of IBA/Fe(110) system.

Keywords: Corrosion inhibitor, 3-indolebutyric acid, Mild steel, EIS, Polarization, Theoretical calculations

1. INTRODUCTION

The corrosion of metals and alloys usually results in huge financial losses and many potential safety issues, and anti-corrosion technology has aroused the great interests of the researchers. One of the most economic and convenient methods was the use of corrosion inhibitors, which can protect metal from corrupting, though used in a very small amount [1-3]. Most of the corrosion inhibitors are organic compounds containing hetero atoms, such as O, N, S, P, unsaturated bonds, or plane conjugated systems [4-6]. When an organic substance containing a group with an unshared electron pair is adsorbed on the surface, a partially charge transfer is achieved between the molecule and metal

and a covalent bond is formed. Generally, the tendency to form a stronger coordination bond and consequently inhibition efficiency was expected to increase in the following order O < N < S < P [7].

Theoretical chemistry has been used recently to explain the mechanism of corrosion inhibition, such as quantum chemical calculations. Recently, density functional theory (DFT) has emerged as a reliable and inexpensive method that is capable of successfully predicting the properties of the chemical systems [8-10]. In addition, as validated by Refs. [11-13], the Metropolis Monte Carlo simulation has been another effective tool to study the interaction of inhibitors with the metal surface or similar problems.

Indole is a heterocyclic compound with a fused structure of the benzene ring with a pyrrole ring. Previous studies have shown that indole [14] and some of its derivatives (such as 5-aminoindole [15, 16], indole-3- carboxylic acid [17], benzotriazole [18], indole-3-acetic acid [19]) display good inhibiting properties on corrosion of steel and copper in different corrosion systems. However, 3-indolebutyric acid (IBA, see Fig. 1) has not been reported as a corrosion inhibitor. The aim of the present work is to study the influence on the inhibition of mild steel corrosion in 0.1 M H_2SO_4 solution using chemical (weight loss), electrochemical techniques (electrochemical impedance spectroscopy and potentiodynamic polarization) as well as molecular simulation methods including Monte Carlo simulation and quantum chemical calculation to explore the adsorption mechanism of IBA molecule on Fe(110) surface.

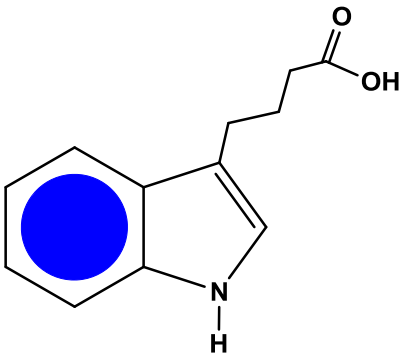

Figure 1. Molecular structure of 3-indolebutyric acid (IBA).

2. EXPERIMENTAL

2.1. Materials and sample preparation

The corrosion tests were performed on mild steel of the following composition: 0.17% C, 0.26% Si, 0.47% Mn, 0.017% S, and the remained is Fe. IBA was dissolved in 0.1 M H_2SO_4 at different concentrations (from 5.0×10^{-4} M to 2.0×10^{-3} M). The solution in the absence of IBA was taken as blank for comparison.

A bulk of mild steel was mechanically cut into 4.0 × 2.0 × 0.5 cm and 1.0 cm × 1.0 cm × 1.0 cm dimensions for weight loss experiments and surface analysis, respectively. For electrochemical

tests, the specimens were embedded in epoxy resin with a geometrical surface area of 1.00 cm^2 exposed to the corrosive medium. The surfaces of all the specimens were polished successively with SiC paper from grade 400 to 1200, then were washed with distilled water, degreased ultrasonically in acetone, dried at room temperature and finally placed in a desiccator.

2.2. Electrochemical test

The electrochemical studies were conducted with CHI604D electrochemical workstation (Shanghai Chenhua CO., LTD) in a traditional three-electrode cell at 25 ± 1 °C. A platinum electrode and a saturated calomel electrode (SCE) with a Luggin capillary were used as auxiliary and reference electrode, respectively. All potentials were referred to SCE reference electrode. Electrochemical impedance spectroscopy (EIS) measurements were carried out at the open circuit potential (E_{OCP}). The alternating current frequency range extended from 10 mHz to 1000 kHz with a 5 mV amplitude. Then the impedance data were analyzed and fitted. The polarization curves were obtained from –250 mV to + 250 mV (*vs.* E_{OCP}) with a 2 mV s^{-1} scan rate. All experiments were performed under atmospheric conditions. Each experiment was repeated at least three times to check the reproducibility.

2.3. Weight loss measurements

Polished and dried steel specimens were immersed in 500 ml of 0.1 M H_2SO_4 solutions for 24 h in the absence and presence of various concentrations of IBA at room temperature. After the immersion period, the steel specimens were withdrawn, carefully rinsed with doubly distilled water, subjected to ultrasonic cleaning in acetone, dried at room temperature, and then weighed. Triplicate experiments were performed in each case, and the mean value of the weight loss was calculated.

2.4. Surface analysis

The surface morphologies of mild steel specimens after immersion in 0.1 M H_2SO_4 solution in the absence and presence of IBA for 24 h were examined by atomic force microscope (AFM). The AFM images were taken using Seiko SPIN 3800 N using non-contact mode, respectively.

2.5. Computational details

The DFT calculations are carried out using the $DMol^3$ code of Accelrys Materials Studio software suite. For the $DMol^3$ calculations, we employ the generalized gradient corrected BLYP functional and the double numerical basis set with polarization functions on hydrogen atoms (DNP) [20]. This approach is shown to yield favorable geometries for a wide variety of systems.

The adsorption progress of IBA molecules on iron surface is investigated by performing Monte Carlo simulations using adsorption locator module. The simulation was carried out in a simulation box (17.3 × 14.9 × 43.1 Å) with periodic boundary conditions in order to simulate a representative part of

an interface devoid of any arbitrary boundary effects. A low energy adsorption site is identified by carrying out a Monte Carlo search of the configurational space of the substrate–adsorbate system as the temperature is slowly decreased (simulated annealing) [21]. This process is repeated to identify further local energy minima. During the course of the simulation, adsorbate molecules are randomly rotated and translated around the substrate. The configuration that results from one of these steps is accepted or rejected according to the selection rules of the Metropolis Monte Carlo method [22]. For the whole simulation procedure, the COMPASS (Condensed-phase Optimized Molecular Potentials for Atomistic Simulation Studies) force field [23] was used to optimize the structures of all components of the system of interest. COMPASS is the first *ab initio* forcefield that enables accurate and simultaneous prediction of chemical properties (structural, conformational, vibrational, *etc.*) and condensed-phase properties (equation of state, cohesive energies, *etc.*) for a broad range of chemical systems. It is also the first high quality forcefield to consolidate parameters of organic and inorganic materials.

3. RESULTS AND DISCUSSION

3.1. Potentiodynamic polarization measurements

It is well known that the spontaneous dissolution of mild steel in acids can be described by the anodic dissolution reaction

$$Fe + 2e^- \rightarrow Fe^{2+} \quad (1)$$

Accompanied by the corresponding cathodic reaction

$$2H^+ + 2e^- \rightarrow H_2 \quad (2)$$

The corrosion of steel in uninhibited acidic solutions is controlled by the hydrogen evolution reaction. Potentiodynamic polarization curves for mild steel in 0.1 M H_2SO_4 solution without and with different concentration IBA are shown in Fig. 2a. The electrochemical parameters, such as corrosion potential (E_{corr}), corrosion current density (i_{corr}), corrosion rate (CR), anodic Tafel slope (β_a), cathodic Tafel slope (β_c) and inhibition efficiency (IE%) are calculated and listed in Table 1. The corrosion rate and inhibition efficiency are defined as follows:

$$CR = \frac{0.129 i_{corr}^0 M}{nd} \quad (3)$$

$$IE\% = \frac{i_{corr}^0 - i_{corr}}{i_{corr}^0} \times 100 \quad (4)$$

where M is the atomic weight of Fe (55.85 g mol^{-1}), n the number of electrons transferred in the metal dissolution (n = 2) and d the density of Fe (7.88 g cm^{-3}). i_{corr}^0 and i_{corr} are the corrosion current densities in the absence and the presence of inhibitor, respectively. The corrosion current densities were obtained by extrapolation of the anodic polarization curves to E_{corr} alone in this study, which was shown in Fig. 2b.

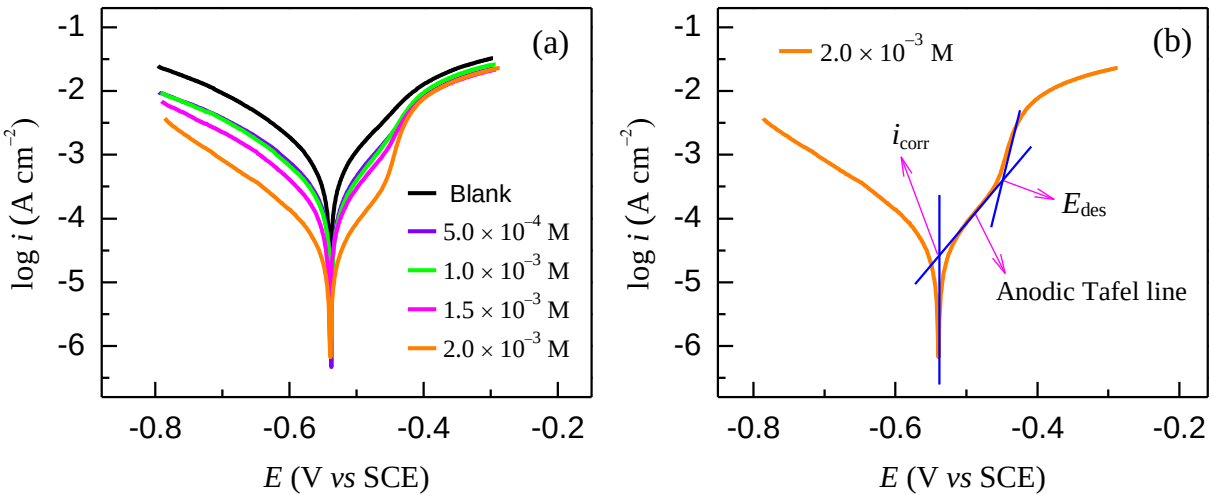

Figure 2. (a) Polarization curves for mild steel in 0.1 M H_2SO_4 without and with different concentrations of IBA; (b) tafel extrapolation of the anodic polarization curve.

From Table 1, it is clear that the values of i_{corr} for mild steel in the inhibited solution were smaller than those for the inhibitor-free solution. This result shows that addition of IBA hindered attack on the steel electrode by acid. Moreover, both cathodic and anodic Tafel branches of the polarization curves (see Fig. 2a) shift towards lower current density values. Thus, IBA can be classified as a mixed-type inhibitor. Specifically, cathodic polarization curves at all given inhibitor concentration display nearly parallel Tafel lines, suggesting that the existence of IBA does not modify the hydrogen reduction mechanism and the cathodic process is activation-controlled [24]. We should note that when the polarization potential shift toward higher over-voltage range, the anodic polarization curves show that the current density increases more remarkable with rising potential. This may be due to the occurrence of significant metal dissolution at a particular potential (this potential can be defined as the desorption potential, E_{des}, see Fig. 2b), which gives rise to the higher desorption rate of the tested inhibitor molecule than its adsorption rate. Similar behaviour have been already reported for other organic inhibitors [25, 26]. The values of anodic and cathodic Tafel slopes (β_a and β_c) are slightly changed indicating that the inhibition mechanism occurred by simple blocking of the available cathodic and anodic sites of the metal surface [27]. It's possible that the adsorption of the acid form of the inhibitor (cations) in outer Helmholtz plane (OHP) leads to a decrease of the potential drop in the outer part of the double layer. This in turn results in a decrease of the concentration of the hydrogen ions in the surface layer and a corresponding increase in the hydrogen evolution overpotential [28].

Table 1. Electrochemical polarization parameters for mild steel in 0.1 M H_2SO_4 solution containing various concentrations of IBA

C (M)	E_{corr} (mV)	i_{corr} (μA cm^{-2})	*CR* (mpy)	β_c (mV dec^{-1})	β_a (mV dec^{-1})	*IE*%
0	–538	644.2	294.49	138.23	89.65	/
5.0×10^{-4}	–538	245.5	112.23	126.72	85.63	61.89
1.0×10^{-3}	–538	188.2	86.03	120.65	83.76	70.78
1.5×10^{-3}	–539	92.5	42.28	118.49	75.58	85.64
2.0×10^{-3}	–539	32.58	14.89	118.25	69.19	94.95

3.2. Electrochemical impedance spectroscopy (EIS)

In order to gain more information about the corrosion inhibition phenomena, EIS measurements was carried out for mild steel in 0.1 M H_2SO_4 solution in the presence and absence of IBA inhibitor. Fig. 3 shows Nyquist plots of the effect of the IBA concentration on the impedance response of mild steel in 0.1 M H_2SO_4 solution. Inspection of the data revealed that the response of the system in the Nyquist complex plane is depressed semicircle which is attributed to the surface inhomogeneity of structural or interfacial origin [29]. It was observed from the Nyquist plots that diameters of these capacitive loops were increasing with increasing inhibitor concentration. This fact revealed that impedance of mild steel against corrosion was increased in accordance with the IBA amount in acid solutions.

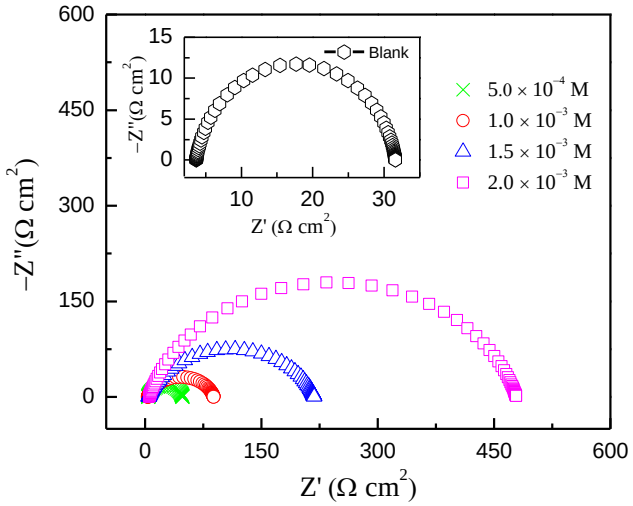

Figure 3. Nyquist diagrams for mild steel in 0.1 M H_2SO_4 containing different concentrations of IBA.

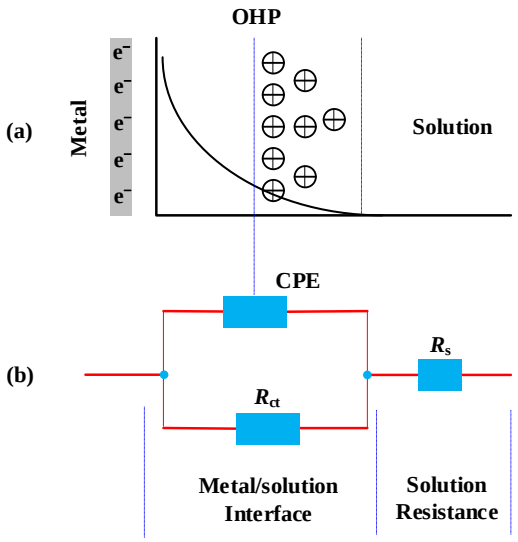

Figure 4. Equivalent circuit used to model impedance data. (OHP: outer Helmholtz plane)

To analyze the impedance spectra of the Nyquist plots, the equivalent circuit model shown in Fig. 4 which we have previously used to analyze mild steel corrosion in H_2SO_4 solutions in the absence and presence of natural products was employed. The circuit employed allows the identification of both solution resistance (R_s) and charge-transfer resistance (R_{ct}). The double layer capacitance (C_{dl}) value is affected by imperfections of the surface which is simulated *via* a constant phase element (CPE) [30]. CPE is constituted of component Y_0 and a coefficient n. It is described by the expression [31]:

$$Z_{CPE} = \frac{1}{Y_0(j\omega)^n} \quad (5)$$

where Y_0 is a proportional factor, j is the imaginary unit, ω is the angular frequency, and n is the deviation parameter which is often related to the surface morphology. Different values of n ($-1 \leq n \leq 1$) give the CPE different electrical component presentation. When n = 0, CPE represents the resistance; n = 1, CPE represents the capacitance; n = –1, CPE represents the inductance; n = 0.5, CPE represents the Warburg impedance [32]. The C_{dl} values were calculated from the equation:

$$C_{dl} = \frac{1}{2\pi f_{max} R_{ct}} \quad (6)$$

where f_{max} is the frequency at which the imaginary component of the impedance is at maximum.

Table 2. Fitted parameters of the equivalent electron circuit

C (M)	R_s (Ω cm^2)	CPE		R_{ct} (Ω cm^2)	C_{dl} (μF cm^{-2})	IE %
		Y_0 ($\times 10^{-5}$ S s^n cm^{-2})	n			
0	3.257	27.65	0.89	27.91	62.89	/
5.0×10^{-4}	4.142	16.47	0.85	54.21	54.62	48.51
1.0×10^{-3}	3.936	12.53	0.85	89.84	43.29	68.93
1.5×10^{-3}	3.374	11.42	0.86	213.5	40.64	86.93
2.0×10^{-3}	4.503	5.353	0.84	484.3	23.92	94.24

The inhibition efficiencies of the inhibitor from EIS were calculated using the following equation:

$$IE\% = \frac{R_{ct} - R_{ct}^0}{R_{ct}} \times 100 \quad (7)$$

where R_{ct} and R_{ct}^0 are the charge transfer resistance in the presence and absence of IBA, respectively. The impedance parameters (such as R_{ct}, R_s, C_{dl}) and IE% are listed in Table 2. It is obvious from the results in the table that the introduction of the different concentrations of IBA into 0.1 M H_2SO_4 solution led to an increase in the charge transfer resistance and a reduction of the double-layer capacitance. Charge transfer resistance was increased from 27.91 (blank) to 484.3 Ω cm^2 (2.0×10^{-3} M), whereas the C_{dl} value decreased from 62.89 to 23.92 μF cm^{-2} for the same inhibitor concentration. The reason for increased R_{ct} can be attributed to decreased heterogeneity of the surface, which was observed probably due to molecular adsorption of the inhibitor at most active sites [33].

The observed decrease in the values of C_{dl} can be explained with the help of the following equation [34]:

$$C_{dl} = \frac{\varepsilon^0 \varepsilon}{d} A \qquad (8)$$

where ε is the local dielectric constant of the medium, ε^0 is the vacuum permittivity, A is the exposure surface, d the thickness of the layer formed at the steel−inhibitor interface. From Eq. (8) it is evident that a decrease in double layer capacitance corresponds to a decrease in local dielectric constant and/or an increase in the thickness of layer formed at the metal−acid interface.

3.3. Weight loss test and the Adsorption behavior

The corrosion rates (v) of steel specimens after 24 h of exposure to 0.1 M H_2SO_4 solution with and without the addition of various concentrations of the investigated inhibitor were calculated, and the obtained data are listed in Table 3. Corrosion rate v (mg cm^{-2} h^{-1}) and the corrosion inhibition efficiency can be obtained by the following formulas:

$$v = \frac{\Delta W}{S \cdot t} \qquad (9)$$

$$IE\% = \frac{v_0 - v_i}{v_0} \times 100 \qquad (10)$$

where ΔW is the average weight loss (mg), S is the surface area of specimens (cm^2), t is the immersion time (h); v_0 and v_i signified the corrosion rate in the absence and presence of inhibitors, respectively. From Table 3, we can see that v decreased while the inhibition efficiency increased with the increasing concentration. And the corrosion rate reached to the minimum at 2.0×10^{-3} M, but the inhibition efficiency reached to maximum. This could be because the inhibitor molecules act by adsorption on the metal surface.

Table 3. Weight loss datas of mild steel in 0.1 M H_2SO_4 solution with different concentrations of IBA for 24h

C (M)	v (mg cm^{-2} h^{-1})	IE%	θ
0	0.6496	/	/
0.5×10^{-4}	0.2673	58.85	0.5885
1.0×10^{-3}	0.1629	74.92	0.7492
1.5×10^{-3}	0.0637	90.19	0.9019
2.0×10^{-3}	0.0333	94.87	0.9487

It is generally accepted that the the adsorption of an organic inhibitor on the surface of a corroding metal may be regarded as a substitution process between the organic compound in aqueous phase and preadsorbed water molecules on the metal/electrolyte interface [35]:

$$Org_{sol} + nH_2O_{ads} \rightarrow Org_{ads} + nH_2O_{sol} \qquad (11)$$

where *n* is the number of water molecules removed from the metal surface for each molecule of inhibitor adsorbed. The adsorption isotherm can give information on the metal–inhibitor interaction. Then, the values of surface coverage, θ, corresponding to different concentrations of inhibitor at 298 K have been used to determine the best adsorption isotherm. The adsorption isotherms generally considered were [36]:

- Temkin isotherm $\exp(f\theta) = K_{ads}C$
- Frumkin isotherm $\frac{\theta}{1-\theta}\exp(-2f\theta) = K_{ads}C$
- Freundluich isotherm $\theta = K_{ads}C$
- Langmuir isotherm $\frac{\theta}{1-\theta} = K_{ads}C$

where K_{ads} is the adsorption equilibrium constant, and f is the factor of energetic inhomogeneity.

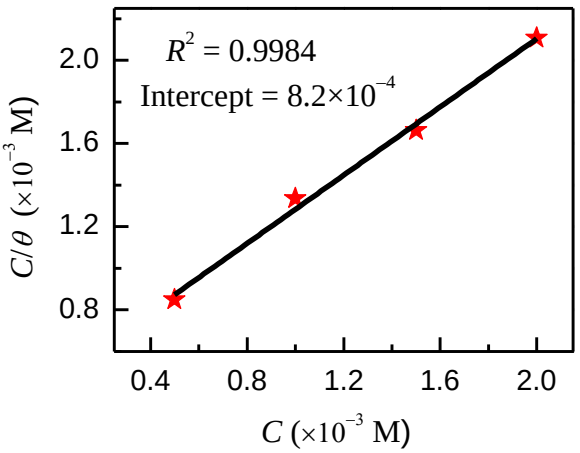

Figure 5. Langmuir adsorption isotherm of IBA on the surface of mild steel.

Experimental results for C/θ versus C yielded straight lines as shown in Fig. 5, which is in agreement with the Langmuir isotherm. When the degree of surface coverage (θ) tends to ~1, a more compact film is formed depending on the molecular structure of the compounds [37]. The linear regression coefficient is almost equal to 1, indicating that IBA molecules formed a single molecule adsorbed layer on the mild steel surface, and there was no interaction between adsorbed molecules.

Gibbs free energy (ΔG_{ads}) could be calculated with the following equation [38]:

$$\Delta G_{ads} = -RT\ln(55.5K_{ads}) \quad (12)$$

where R is the gas constant (8.314 J K^{-1} mol^{-1}), T was the absolute temperature (K), and the value 55.5 is the molecular concentration of water in solution expressed in mol L^{-1}. In Fig. 5, the intercept on the vertical axis is the value of $1/K_{ads}$, which is 8.2 × 10^{-4}. Then according to Eq. (12), we calculated the ΔG_{ads} = −27.57 kJ mol^{-1}. The negative values of ΔG_{ads} indicated that the adsorption of IBA in 0.1 M H_2SO_4 was a spontaneous process.

3.4. AFM analysis

Surface morphology of the mild steel specimens was investigated in 0.1 M H_2SO_4 solutions in the absence and presence of inhibitor through AFM technique. The two/three-dimensional AFM images are shown in Fig. 6. The average roughness of polished mild steel (Fig. 6a) and mild steel in 0.1 M H_2SO_4 without inhibitor (Fig. 6b) was calculated as 86 nm and 843 nm, respectively. It is clearly shown in Fig. 6b that mild steel sample is rough due to the acid attack. However, in the presence of optimum concentration of inhibitor the average roughness was reduced to 163 nm, and shown in Fig. 6c. This indicates the less attack of acid due to formation of adsorbed inhibitor film over the surface of mild steel.

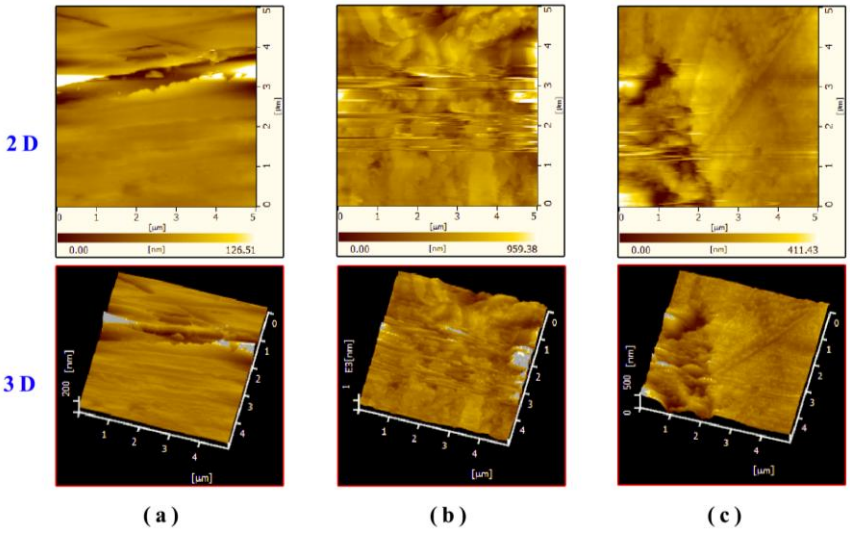

Figure 6. 2D/3D AFM micrographs of (a) freshly polished mild steel specimen, (b) the specimen immersed in 0.1 M H_2SO_4 solution for 24 h, (c) with 2.0×10^{-3} IBA inhibitor.

3.5. Theory study

The deprotonated form of IBA stems from the following reaction in solution:

$$C_{11}H_{12}NCOOH_{(aq)} \leftrightarrow C_{11}H_{12}NCOO^{-}_{(aq)} + H^{+}_{(aq)} \qquad (13)$$

The pKa constant for this reaction is 4.86 (calculated from ACD/Labs). This implies that, at lower pH, the IBA molecule is predominantly in neutral form, but as pH increases, the percentage of deprotonated molecules increases. For simplicity sake, we just consider the neutral molecule in the following discussions.

3.5.1 Quantum chemical calculations

The optimized geometry structure, the density distribution of frontier molecular orbitals (HOMO and LUMO) as well as the electrostatic potential (ESP) of IBA molecule are presented in Fig.

7. The selected quantum chemical parameters such as E_{HOMO}, E_{LUMO}, molecular dipole moment μ, the fraction of electrons transferred from the inhibitor to iron surface (ΔN), are collected in Table 4. The spatial distribution of the HOMO and the LUMO are important for understanding the adsorption preferences of IBA. Obviously, HOMO is distributed on the indole ring, implying that the preferred sites for electrophilic attack of IBA would be of the five-membered ring as well as the benzene ring. On the other hand, the LUMO orbitals, which can accept electrons from the metal using π* orbitals to form π-back bonds, are saturated around the carboxylic acid group. For the ESP map, the negatively charged red regions are near the ring and oxygen atoms. These electron-rich areas would be preferred sites for adsorption to metal surfaces.

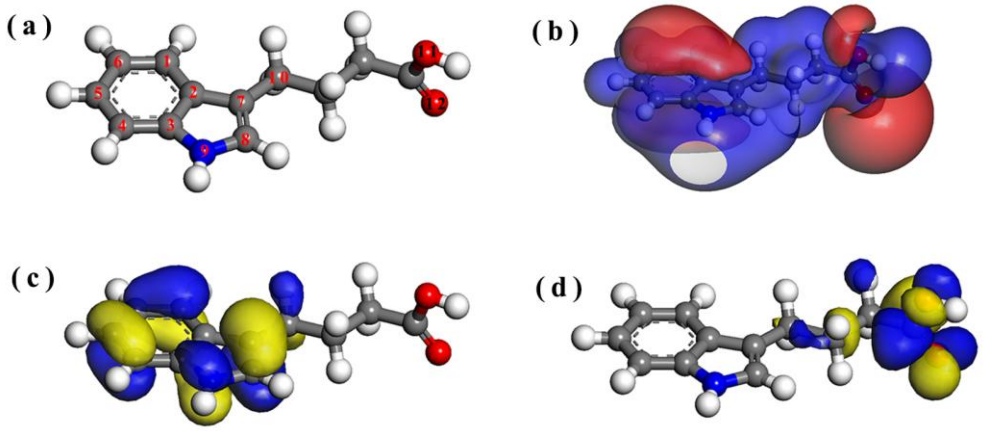

Figure 7. Optimized structure (a) and electronic properties of the IBA molecule: (b) electrostatic potential, (c) HOMO orbital, and (d) LUMO orbital.

Table 4. Calculated atomic charges (q), Fukui functions, and some global reactivity parameters for IBA[a]

	C1	C2	C3	C4	C5	C6	C7	C8	N9	C10	O11	O12
q	−0.054	−0.027	0.029	−0.065	−0.055	−0.059	−0.029	−0.026	−0.077	−0.042	−0.180	−0.285
f^+	0.063	0.024	0.019	0.068	0.057	0.041	0.023	0.056	0.025	0.009	0.061	0.111
f^-	0.080	0.020	0.023	0.074	0.075	0.058	0.103	0.091	0.080	0.015	0.008	0.019
E_{HOMO} = −4.726 eV E_{LUMO} = −1.053 eV ΔE = 3.673 eV μ = 2.264 Debye ΔN = 1.119												

[a] The atom numbering is given in Fig. 7a.

The local reactivity of the IBA molecule was analyzed through an evaluation of the Fukui indices [39]. The Fukui function f_k is motivated by the fact that if an electron δ is transferred to an N electron molecule, it will tend to distribute so as to minimize the energy of the resulting $N + \delta$ electron system [40]. It is defined as the first derivative of the electronic density ($\rho(\vec{r})$) with respect to the number of electrons N in a constant external potential $v(\vec{r})$.

$$f_k = \left(\frac{\partial \rho(\vec{r})}{\partial N} \right)_{v(\vec{r})} \qquad (14)$$

$$f_k^+ = q_k(N+1) - q_k(N) \quad \text{(for nucleophilic attack)} \qquad (15)$$

$$f_k^- = q_k(N) - q_k(N-1) \quad \text{(for nucleophilic attack)} \qquad (16)$$

Herein, $q_k(N+1)$, $q_k(N)$, and $q_k(N-1)$ represent the atomic charges of the anionic, neutral, and cationic species, respectively. The condensed Fukui functions were obtained through the finite difference approximation using Hirshfeld population analysis. Based on the data in Table 4, it is evident that the preferred sites for nucleophilic/ electrophilic attack in IBA are near oxygen and heteroatoms, respectively. These results are basically consistent with previous HOMO/LUMO analysis.

3.5.2 Monte Carlo simulation

Using *x*:*y* = 3:10 (as defined in Table 5) modeling as an example, the total energy, average total energy, van der Waals energy, electrostatic energy and intramolecular energy for IBA/H_2O/Fe(110) surface were calculated by optimizing the whole system and presented in Fig. 8a. The Monte Carlo simulation process tries to find the lowest energy for the whole system. The structures of the adsorbate components are minimized until they satisfy certain specified criteria. The most stable configuration for adsorption of pure water molecules on iron substrate is presented in the left panel of Fig. 9. A water monolayer was formed close to the metal surface. This is can be seen as the microcosmic causation for metal corrosion.

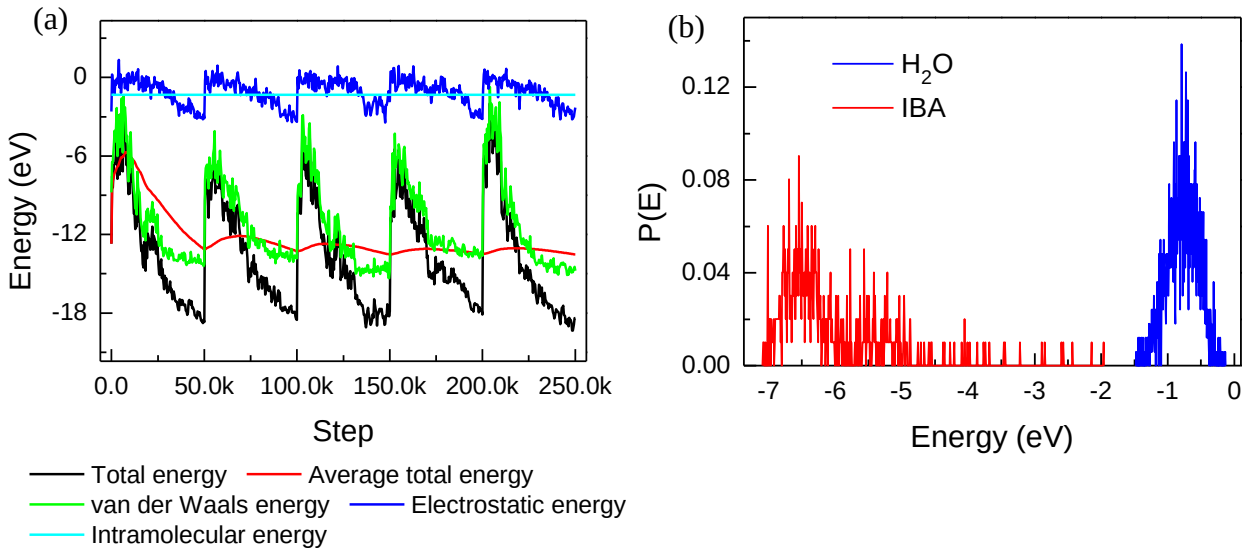

Figure 8. (a) Total energy distribution for IBA/H_2O/Fe(110) system during energy optimization process; (b) the adsorption energy distribution of the adsorbates (IBA and H_2O) on Fe(110). (*x*:*y* = 3:10)

The outputs and descriptors calculated by the Monte Carlo simulation are presented in Table 5. The parameters include total energy of the substrate–adsorbate configuration, which is defined as the

sum of the energies of the adsorbate components, the rigid adsorption energy, and the deformation energy. The substrate energy (iron surface) is taken as zero.

Table 5. Outputs and descriptors calculated by the Mont Carlo simulation for adsorption of IBA on Fe(110) (in eV)

IBA:H_2O[a]	Total energy	Adsorption energy	Rigid adsorption	Deformation energy	H_2O: dE_{ad}/dN_i	IBA: dE_{ad}/dN_i
1:10	−13.03	−12.59	−12.47	−0.12	−0.77	−6.37
2:10	−19.14	−18.27	−17.68	−0.59	−0.60	−6.68
3:10	−23.81	−22.49	−21.72	−0.78	−0.47	−6.45

[a] IBA:H_2O = *x*:*y* means the adsorbates contain *x* IBA molecules and *y* water molecules.

Besides, adsorption energy reports the energy released (or required) when the relaxed adsorbate component was adsorbed on the substrate. The adsorption energy is defined as the sum of the rigid adsorption energy and the deformation energy for the adsorbate component. The rigid adsorption energy reports the energy released (or required) when the unrelaxed adsorbate component (before the geometry optimization step) was adsorbed on the substrate. The deformation energy reports the energy released when the adsorbed adsorbate component was relaxed on the substrate surface. Table 5 also gives (dE_{ad}/dN_i), which reports the energy of substrate–adsorbate configurations where one of the adsorbate component has been removed. As can be seen from Table 5, adsorbate molecules show high adsorption energy during the simulation process, and the adsorption energy increases as the number of IBA molecules increases. This indicates that IBA molecules are possible efficient inhibitor. A representative adsorption energy distribution of the adsorbates (IBA and H_2O) on Fe(110) is presented in Fig. 8b. It is easy to see that IBA molecules display a greater adsorption energy than H_2O. Consequently, a gradual substitution process occurs, just as the Eq. (11) implies. Eventually, as can be seen from the right panel of Fig. 9, the IBA molecule is preferentially oriented parallel to the surface in order to maximize contact and hence augment the degree of surface coverage. It is likely to adsorb on the iron surface to form a stable hydrophobic layer and protect iron from corrosion.

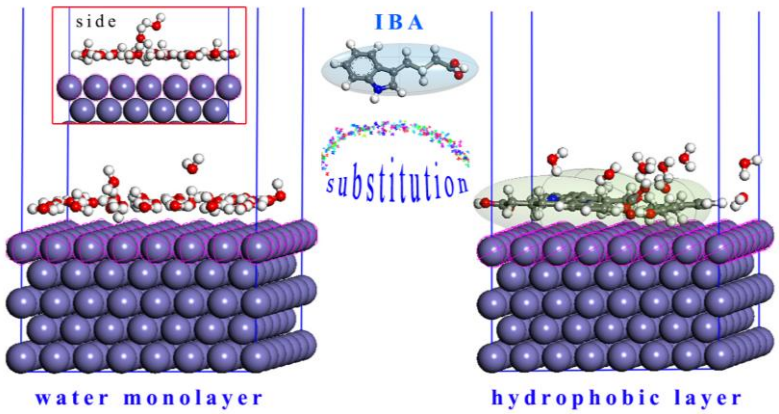

Figure 9. Mode of the adsorption process of IBA on Fe(110).

4. CONCLUSIONS

The inhibition behavior of IBA on mild steel in 0.1 M H_2SO_4 was investigated using different techniques. The following points can be highlighted:

1) IBA acts as a good inhibitor for the corrosion of mild steel in 0.1 M H_2SO_4 and its inhibition efficiency is concentration dependent.

2) The potentiodynamic polarization curves show that IBA prevents metal dissolution and also hydrogen evolution reactions.

3) The adsorption of IBA on the surface of mild steel in 0.1 M H_2SO_4 follows a Langmuir adsorption isotherm. The high value of K_{ads} and negative value of ΔG_{ads} suggested that the adsorption process is a spontaneous, exothermic process.

4) AFM micrographs show a smoother surface for inhibited metal samples than uninhibited samples due to the formation of a thin film.

5) The Monte Carlo simulation suggests that IBA molecules adsorb on Fe(110) surface in a planar manner with a high negative adsorption energy.

ACKNOWLEDGEMENTS
This research was sponsored by the National Natural Science Foundation of China (21376282).

References

1. B.E.A. Rani, B.B.J. Basu, *Int. J. Corros.* 2012 (2012) 1.
2. M. Finšgar, J. Jackson, *Corros. Sci.* 86 (2014) 17.
3. M.M. Antonijevic, M.B. Petrovic, *Int. J. Electrochem. Sci.* 3 (2008) 1.
4. M. Finsgar, A. Lesar, A. Kokalj, I. Milosev, *Electrochim. Acta* 53 (2008) 8287.
5. K.F. Khaled, N.S. Abdelshafi, A.A. El-Maghraby, A. Aouniti, N. Al-Mobarak, B. Hammouti, *Int. J. Electrochem. Sci.* 7 (2012) 12706.
6. F. Bentiss, M. Lagrenee, M. Traisnel, J.C. Hornez, *Corros. Sci.* 41 (1999) 789.
7. I. Lukovits, E. Kalman, F. Zucchi, *Corrosion* 57 (2001) 3.
8. G. Gece, *Corros. Sci.* 50 (2008) 2981.
9. N. Kovačević, A. Kokalj, *Corros. Sci.* 73 (2013) 7.
10. L. Guo, W. Dong, S. Zhang, *RSC Adv.* 4 (2014) 41956.
11. K.F. Khaled, *Appl. Surf. Sci.* 256 (2010) 6753.
12. K.F. Khaled, A. El-Maghraby, *Arab. J. Chem.* 7 (2014) 319.
13. S.R. Jale, M. Bulow, F.R. Fitch, N. Perelman, D. Shen, *J. Phys. Chem. B* 104 (2000) 5272.
14. M. Dudukcu, B. Yazici, M. Erbil, *Mater. Chem. Phys.* 87 (2004) 138.
15. G. Moretti, G. Quartarone, A. Tassan, A. Zingales, *Electrochim. Acta* 41 (1996) 1971.
16. M. Dudukcu, *Mater. Corros.* 62 (2011) 264.
17. G. Quartarone, M. Battilana, L. Bonaldo, T. Tortato, *Corros. Sci.* 50 (2008) 3467.
18. K.F. Khaled, *Mater. Chem. Phys.* 112 (2008) 290.
19. G. Avci, *Colloids Surf., A* 317 (2008) 730.
20. A.D. Becke, *J. Chem. Phys.* 88 (1988) 2547.
21. S. Kirkpatrick, C.D. Gelatt, M.P. Vecchi, *Science* 220 (1983) 671.
22. N. Metropolis, A.W. Rosenbluth, M.N. Rosenbluth, A.H. Teller, E. Teller, *J. Chem. Phys.* 21 (1953) 1087.

23. H. Sun, P. Ren, J.R. Fried, *Comput. Theor. Polym. Sci.* 8 (1998) 229.
24. F. Bentiss, M. Traisnel, L. Gengembre, M. Lagrenée, *Appl. Surf. Sci.* 152 (1999) 237.
25. F. Bentiss, F. Gassama, D. Barbry, L. Gengembre, H. Vezin, M. Lagrenee, M. Traisnel, *Appl. Surf. Sci.* 252 (2006) 2684.
26. A. El Bribri, M. Tabyaoui, B. Tabyaoui, H. El Attari, E. Bentiss, *Mater. Chem. Phys.* 141 (2013) 240.
27. N. Missoum, A. Guendouz, N. Boussalah, B. Hammouti, A. Chetouani, M. Taleb, A. Aouniti, S. Ghalem, *Res. Chem. Intermed.* 39 (2013) 3441.
28. K.F. Khaled, *J. Solid State Electrochem.* 13 (2009) 1743.
29. S.S.A. El Rehim, M.A. Amin, S.O. Moussa, A.S. Ellithy, *Mater. Chem. Phys.* 112 (2008) 898.
30. Y. Gonzalez, M.C. Lafont, N. Pebere, G. Chatainier, J. Roy, T. Bouissou, *Corros. Sci.* 37 (1995) 1823.
31. E.E. Ebenso, M.M. Kabanda, L.C. Murulana, A.K. Singh, S.K. Shukla, *Ind. Eng, Chem, Res.* 51 (2012) 12940.
32. M.M. Kabanda, S.K. Shukla, A.K. Singh, L.C. Murulana, E.E. Ebenso, *Int. J. Electrochem. Sci.* 7 (2012) 8813.
33. M. Lebrini, M. Lagrenee, H. Vezin, M. Traisnel, F. Bentiss, *Corros. Sci.* 49 (2007) 2254.
34. F. Bentiss, M. Lebrini, H. Vezin, M. Lagrenee, *Mater. Chem. Phys.* 87 (2004) 18.
35. S. Vishwanatham, P.K. Sinha, *Anti-Corros. Method. M.* 56 (2009) 139.
36. A. Anejjar, A. Zarrouk, R. Salghi, D. Ben Hmamou, H. Zarrok, S.S. Al-Deyab, M. Bouachrine, B. Hammouti, N. Benchat, *Int. J. Electrochem. Sci.* 8 (2013) 5961.
37. D. Ben Hmamou, R. Salghi, A. Zarrouk, M.R. Aouad, O. Benali, H. Zarrok, M. Messali, B. Hammouti, M.M. Kabanda, M. Bouachrine, E.E. Ebenso, *Ind. Eng, Chem, Res.* 52 (2013) 14315.
38. Y. Marcus, *J. Chem. Soc., Faraday Trans.* 87 (1991) 2995.
39. W. Yang, W.J. Mortier, *J. Am. Chem. Soc.* 108 (1986) 5708.
40. P. Thanikaivelan, J. Padmanabhan, V. Subramanian, T. Ramasami, *Theor. Chem. Acc.* 107 (2002) 326.

© 2015 The Authors. Published by ESG (www.electrochemsci.org). This article is an open access article distributed under the terms and conditions of the Creative Commons Attribution license (http://creativecommons.org/licenses/by/4.0/).